

## Supplementary information

### Non-invasive sensing of transepithelial barrier function and tissue differentiation in organs-on-chips using impedance spectroscopy

Marinke W. van der Helm,<sup>a,†</sup> Olivier Y.F. Henry,<sup>b,†</sup> Amir Bein,<sup>b</sup> Tiama Hamkins-Indik,<sup>b</sup> Michael J. Cronce,<sup>b</sup> William D. Leineweber,<sup>b</sup> Mathieu Odijk,<sup>a</sup> Andries D. van der Meer,<sup>c</sup> Jan C.T. Eijkel,<sup>a</sup> Donald E. Ingber,<sup>b,d,e</sup> Albert van den Berg<sup>a</sup> and Loes I. Segerink<sup>a</sup>

---

<sup>a</sup> BIOS Lab on a Chip group, MESA+ Institute for Nanotechnology, MIRA Institute for Biomedical Technology and Technical Medicine and Max Planck Center for Complex Fluid Dynamics, University of Twente, P. O. Box 217, 7500 AE Enschede, the Netherlands. E-mail: [l.i.segerink@utwente.nl](mailto:l.i.segerink@utwente.nl)

<sup>b</sup> Wyss Institute for Biologically Inspired Engineering at Harvard University, CLSB Bldg. 5th floor, 3 Blackfan Circle, Boston, MA 02115, USA. E-mail: [olivier.henry@wyss.harvard.edu](mailto:olivier.henry@wyss.harvard.edu)

<sup>c</sup> Applied Stem Cell Technology, MIRA Institute for Biomedical Technology and Technical Medicine, University of Twente, P. O. Box 217, 7500 AE Enschede, the Netherlands

<sup>d</sup> Vascular Biology Program and Department of Surgery, Boston Children's Hospital and Harvard Medical School, Boston, MA 02115, USA

<sup>e</sup> Harvard John A. Paulson School of Engineering and Applied Sciences, Harvard University, Cambridge, MA 02138, USA

† These authors contributed equally to this work

Key words: organ-on-chip, transepithelial electrical resistance, TEER, impedance spectroscopy, gut epithelium, villi formation, gut-on-a-chip

---

## Supplementary theory 1: Theory of solving (large) electrical networks

Suppose a network with 9 nodes (labeled A-I) oriented in a 3-by-3 configuration, all connected horizontally and vertically by resistors (Fig. ST1). At node A an input current is applied. Node I is connected to ground, serving as reference node with a potential of 0 V. Furthermore, all horizontal resistors are equal:  $R_1 = R_2 = R_6 = R_7 = R_{11} = R_{12} = R_h$ . Also, all vertical resistors are equal:  $R_3 = R_4 = R_5 = R_8 = R_9 = R_{10} = R_v$ . The directions of the currents through all resistors are marked in the image.

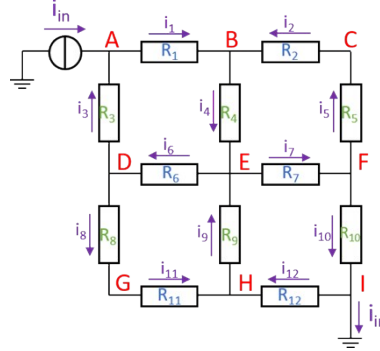


Fig ST1 Network consisting of 9 nodes, all connected horizontally and vertically by resistors.

Kirchhoff's current law states that the sum of the currents in each node should equal 0 A. So for all nodes this results in:

$$\begin{aligned}
 \text{A: } & i_{in} + i_3 - i_1 = 0 \\
 \text{B: } & i_1 + i_2 - i_4 = 0 \\
 \text{C: } & i_5 - i_2 = 0 \\
 \text{D: } & i_6 - i_3 - i_8 = 0 \\
 \text{E: } & i_4 + i_9 - i_6 - i_7 = 0 \\
 \text{F: } & i_7 - i_5 - i_{10} = 0 \\
 \text{G: } & i_8 - i_{11} = 0 \\
 \text{H: } & i_{11} + i_{12} - i_9 = 0 \\
 \text{I: } & i_{10} - i_{12} - i_{in} = 0
 \end{aligned}$$

When the branch currents are expressed in node voltages and resistances following Ohm's law:

$$\begin{aligned}
 \text{A: } & i_{in} + \frac{u_D - u_A}{R_3} - \frac{u_A - u_B}{R_1} = 0 \\
 \text{B: } & \frac{u_A - u_B}{R_1} + \frac{u_C - u_B}{R_2} - \frac{u_B - u_E}{R_4} = 0 \\
 \text{C: } & \frac{u_F - u_C}{R_5} - \frac{u_C - u_B}{R_2} = 0 \\
 \text{D: } & \frac{u_E - u_D}{R_6} - \frac{u_D - u_A}{R_3} - \frac{u_D - u_G}{R_8} = 0 \\
 \text{E: } & \frac{u_B - u_E}{R_4} + \frac{u_H - u_E}{R_9} - \frac{u_E - u_D}{R_6} - \frac{u_E - u_F}{R_7} = 0 \\
 \text{F: } & \frac{u_E - u_F}{R_7} - \frac{u_F - u_C}{R_5} - \frac{u_F - u_I}{R_{10}} = 0 \\
 \text{G: } & \frac{u_D - u_G}{R_8} - \frac{u_G - u_H}{R_{11}} = 0 \\
 \text{H: } & \frac{u_G - u_H}{R_{11}} + \frac{u_I - u_H}{R_{12}} - \frac{u_H - u_E}{R_9} = 0 \\
 \text{I: } & \frac{u_F - u_I}{R_{10}} - \frac{u_I - u_H}{R_{12}} - i_{in} = 0
 \end{aligned}$$

Rewriting the equations and filling in  $R_h$  and  $R_v$  yields:

$$\text{A: } i_{in} = u_A \left( \frac{1}{R_1} + \frac{1}{R_3} \right) - \frac{u_D}{R_3} - \frac{u_B}{R_1} = u_A \left( \frac{1}{R_h} + \frac{1}{R_v} \right) - \frac{u_B}{R_h} - \frac{u_D}{R_v}$$

$$\begin{aligned}
\text{B: } 0 &= u_B \left( \frac{1}{R_1} + \frac{1}{R_2} + \frac{1}{R_4} \right) - \frac{u_A}{R_1} - \frac{u_C}{R_2} - \frac{u_E}{R_4} = u_B \left( \frac{2}{R_h} + \frac{1}{R_v} \right) - \frac{u_A}{R_h} - \frac{u_C}{R_h} - \frac{u_E}{R_v} \\
\text{C: } 0 &= u_C \left( \frac{1}{R_5} + \frac{1}{R_2} \right) - \frac{u_F}{R_5} - \frac{u_B}{R_2} = u_C \left( \frac{1}{R_v} + \frac{1}{R_h} \right) - \frac{u_F}{R_v} - \frac{u_B}{R_h} \\
\text{D: } 0 &= u_D \left( \frac{1}{R_6} + \frac{1}{R_3} + \frac{1}{R_8} \right) - \frac{u_E}{R_6} - \frac{u_A}{R_3} - \frac{u_G}{R_8} = u_D \left( \frac{1}{R_h} + \frac{2}{R_v} \right) - \frac{u_E}{R_h} - \frac{u_A}{R_v} - \frac{u_G}{R_v} \\
\text{E: } 0 &= u_E \left( \frac{1}{R_4} + \frac{1}{R_9} + \frac{1}{R_6} + \frac{1}{R_7} \right) - \frac{u_B}{R_4} - \frac{u_H}{R_9} - \frac{u_D}{R_6} - \frac{u_F}{R_7} = u_E \left( \frac{2}{R_v} + \frac{2}{R_h} \right) - \frac{u_B}{R_v} - \frac{u_H}{R_v} - \frac{u_D}{R_h} - \frac{u_F}{R_h} \\
\text{F: } 0 &= u_F \left( \frac{1}{R_7} + \frac{1}{R_5} + \frac{1}{R_{10}} \right) - \frac{u_E}{R_7} - \frac{u_C}{R_5} - \frac{u_I}{R_{10}} = u_F \left( \frac{1}{R_h} + \frac{2}{R_v} \right) - \frac{u_E}{R_h} - \frac{u_C}{R_v} - \frac{u_I}{R_v} \\
\text{G: } 0 &= u_G \left( \frac{1}{R_8} + \frac{1}{R_{11}} \right) - \frac{u_D}{R_8} - \frac{u_H}{R_{11}} = u_G \left( \frac{1}{R_v} + \frac{1}{R_h} \right) - \frac{u_D}{R_v} - \frac{u_H}{R_h} \\
\text{H: } 0 &= u_H \left( \frac{1}{R_{11}} + \frac{1}{R_{12}} + \frac{1}{R_9} \right) - \frac{u_G}{R_{11}} - \frac{u_I}{R_{12}} - \frac{u_E}{R_9} = u_H \left( \frac{2}{R_h} + \frac{1}{R_v} \right) - \frac{u_G}{R_h} - \frac{u_I}{R_h} - \frac{u_E}{R_v} \\
\text{I: } -i_{in} &= u_I \left( \frac{1}{R_{10}} + \frac{1}{R_{12}} \right) - \frac{u_F}{R_{10}} - \frac{u_H}{R_{12}} = u_I \left( \frac{1}{R_v} + \frac{1}{R_h} \right) - \frac{u_F}{R_v} - \frac{u_H}{R_h}
\end{aligned}$$

The resulting system of equations can also be written in matrix form:

$$\begin{bmatrix}
\frac{1}{R_h} + \frac{1}{R_v} & -\frac{1}{R_h} & 0 & -\frac{1}{R_v} & 0 & 0 & 0 & 0 & 0 \\
-\frac{1}{R_h} & \frac{2}{R_h} + \frac{1}{R_v} & -\frac{1}{R_h} & 0 & -\frac{1}{R_v} & 0 & 0 & 0 & 0 \\
0 & -\frac{1}{R_h} & \frac{1}{R_h} + \frac{1}{R_v} & 0 & 0 & -\frac{1}{R_v} & 0 & 0 & 0 \\
-\frac{1}{R_v} & 0 & 0 & \frac{1}{R_h} + \frac{2}{R_v} & -\frac{1}{R_h} & 0 & -\frac{1}{R_v} & 0 & 0 \\
0 & -\frac{1}{R_v} & 0 & -\frac{1}{R_h} & \frac{2}{R_h} + \frac{2}{R_v} & -\frac{1}{R_h} & 0 & -\frac{1}{R_v} & 0 \\
0 & 0 & -\frac{1}{R_v} & 0 & -\frac{1}{R_h} & \frac{1}{R_h} + \frac{2}{R_v} & 0 & 0 & -\frac{1}{R_v} \\
0 & 0 & 0 & -\frac{1}{R_v} & 0 & 0 & \frac{1}{R_h} + \frac{1}{R_v} & -\frac{1}{R_h} & 0 \\
0 & 0 & 0 & 0 & -\frac{1}{R_v} & 0 & -\frac{1}{R_h} & \frac{2}{R_h} + \frac{1}{R_v} & -\frac{1}{R_h} \\
0 & 0 & 0 & 0 & 0 & -\frac{1}{R_v} & 0 & -\frac{1}{R_h} & \frac{1}{R_h} + \frac{1}{R_v}
\end{bmatrix}
\cdot
\begin{bmatrix}
u_A \\
u_B \\
u_C \\
u_D \\
u_E \\
u_F \\
u_G \\
u_H \\
u_I
\end{bmatrix}
=
\begin{bmatrix}
0 \\
0 \\
0 \\
0 \\
0 \\
0 \\
0 \\
0 \\
0
\end{bmatrix}$$

As node **I** is the reference node,  $u_I = 0$  can be filled in and the right column of the matrix can be omitted. Then, to prevent having an overdetermined system, the equation corresponding to reference node **I** (bottom row) can also be omitted in this matrix:

$$\begin{bmatrix}
\frac{1}{R_h} + \frac{1}{R_v} & -\frac{1}{R_h} & 0 & -\frac{1}{R_v} & 0 & 0 & 0 & 0 \\
-\frac{1}{R_h} & \frac{2}{R_h} + \frac{1}{R_v} & -\frac{1}{R_h} & 0 & -\frac{1}{R_v} & 0 & 0 & 0 \\
0 & -\frac{1}{R_h} & \frac{1}{R_h} + \frac{1}{R_v} & 0 & 0 & -\frac{1}{R_v} & 0 & 0 \\
-\frac{1}{R_v} & 0 & 0 & \frac{1}{R_h} + \frac{2}{R_v} & -\frac{1}{R_h} & 0 & -\frac{1}{R_v} & 0 \\
0 & -\frac{1}{R_v} & 0 & -\frac{1}{R_h} & \frac{2}{R_h} + \frac{2}{R_v} & -\frac{1}{R_h} & 0 & -\frac{1}{R_v} \\
0 & 0 & -\frac{1}{R_v} & 0 & -\frac{1}{R_h} & \frac{1}{R_h} + \frac{2}{R_v} & 0 & 0 \\
0 & 0 & 0 & -\frac{1}{R_v} & 0 & 0 & \frac{1}{R_h} + \frac{1}{R_v} & -\frac{1}{R_h} \\
0 & 0 & 0 & 0 & -\frac{1}{R_v} & 0 & -\frac{1}{R_h} & \frac{2}{R_h} + \frac{1}{R_v}
\end{bmatrix}
\cdot
\begin{bmatrix}
u_A \\
u_B \\
u_C \\
u_D \\
u_E \\
u_F \\
u_G \\
u_H
\end{bmatrix}
=
\begin{bmatrix}
0 \\
0 \\
0 \\
0 \\
0 \\
0 \\
0 \\
0
\end{bmatrix}$$

This can be summarized as:

$$G \cdot U = I$$

Here  $G$  is a matrix containing the conductivities (which is the inverse of resistances) between all nodes,  $U$  is a vector containing the potentials in these nodes and  $I$  is a vector with the currents imposed onto these nodes.

To directly produce such a matrix describing the system of equations of any (large) electrical network, the following patterns or rules can be followed, as recognized in this matrix:

- The matrix eventually has an equal number of rows and columns, both equaling the total number of nodes minus 1.
- When two nodes  $i$  and  $j$  are connected, in the matrix at place  $G(i,j)$  and  $G(j,i)$  the negative conductance between the nodes is filled in:  $G(i,j) = G(j,i) = -1/R_{ij}$ . If two nodes  $i$  and  $k$  are not connected, the conductivity between these nodes is 0:  $G(i,k) = G(k,i) = 0$ . The matrix is thus symmetrical in the main diagonal. In addition, capacitors can also be described in such a conductance matrix as their conductance is  $G_C = j\omega C$ .
- On the main diagonal the negative sum of each row is inserted:  $G(i,i) = -G(i,j) - G(i,k) - \dots$ .

## Supplementary theory 2: Sensitivity distributions

In four-terminal resistance measurements, electric fields and current densities develop in 3D space, resulting in different contributions of separate volume elements to the final measured resistance.<sup>1</sup> Theory for resistance extraction from such four-terminal measurements was developed by Geselowitz,<sup>2</sup> and was recently summarized by Wang *et al.*<sup>3</sup> Geselowitz's approach starts by mapping the pattern of current flow between the current carrying electrodes. At every location in the measured volume, the current flow is described by the current density  $J$  (A/m<sup>2</sup>): a vector quantity with magnitude and direction. The local current density gives rise to a local electrical field, which is also a vector quantity, dependent on the local electrical resistivity. Geselowitz shows that this generated field is picked up the strongest by the readout electrodes, when this field is exactly in line with the field that would exist when the same current was sent through the readout electrodes instead of through the excitation electrodes (shown schematically in **Fig ST2**). The interchangeability of the excitation and readout electrode pairs is Geselowitz's reciprocity theorem. On the basis of this theorem, later authors calculated a sensitivity coefficient for every small volume element, quantifying the extent to which it contributes to the total measured impedance.<sup>1, 4</sup> As this sensitivity coefficient is thus based on the extent to which the generated and measured fields of vectors line up, it contains the dot product of two vectors. Grimnes and Martinsen<sup>1</sup> calculated the sensitivity coefficient based on the dot product of the current densities, while, as another option, Metherall *et al.*<sup>4</sup> had used the dot product of the developed electric fields in earlier work. In this paper we follow the formulation of Grimnes *et al.* for the sensitivity coefficient  $S$ :

$$S = \frac{J_1 \cdot J_2}{i^2} \quad (\text{ST2-1})$$

In this equation,  $J_1$  is the current density vector (A/m<sup>2</sup>) in each volume element when a current  $i$  (A) is injected between the two excitation electrodes.  $J_2$  is the current density when  $i$  is injected between the two readout electrodes.<sup>1</sup> The higher the value for the sensitivity coefficient, the more a change in the resistivity of this volume element will affect the total resistance. A negative sensitivity means that an increase in the resistivity of this volume element will, maybe surprisingly but not counterintuitively, result in a lower total measured resistance.

Geselowitz<sup>2</sup>, Metherall<sup>4</sup> and Grimnes<sup>1</sup> *et al.* only considered resistive behavior in the measured volume, and not the case where (some of) the charge is capacitively stored in the measured volume. Capacitive charging, however, will occur across the cell layer during impedance spectroscopy because of the capacitive behavior of cell membranes.<sup>5</sup> <sup>6</sup> The sensitivity coefficient equally applies to such a case, as the current densities in **Eq. ST2** can be written as the sum of a conductive current density  $\sigma E$ , and a capacitive charging current density  $\epsilon dE/dt$ :

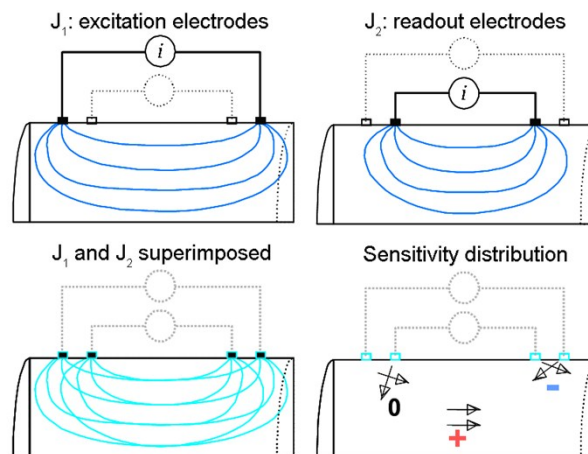


**Fig. ST2** | Schematic illustration of the sensitivity distribution of four-terminal impedance sensing in a uniformly conductive cylinder. The electrical field arising when current is applied between the excitation electrodes is superimposed on the electric field arising when the same current is applied between the readout electrodes (following the reciprocity theorem). Where the fields align, the resulting sensitivity is high; where the fields are perpendicular the

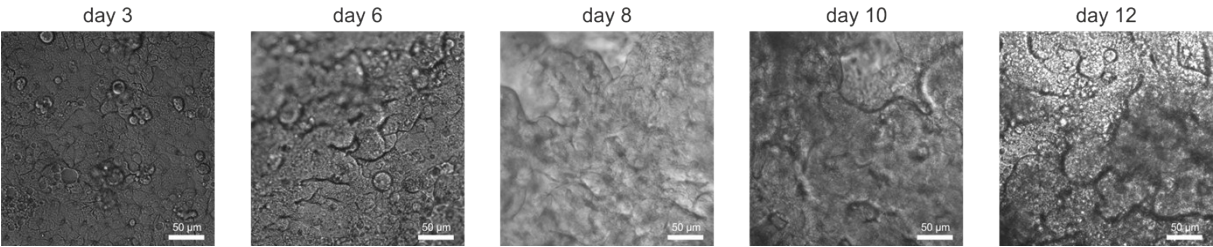
$$S = \frac{J_1 \cdot J_2}{i^2} = \frac{\left(\sigma E_1 + \epsilon \frac{dE_1}{dt}\right) \cdot \left(\sigma E_2 + \epsilon \frac{dE_2}{dt}\right)}{i^2} \quad (\text{ST2-2})$$

In this equation,  $E$  is the electric field vector (V/m),  $\sigma$  is the conductivity (S/m) and  $\epsilon$  is the permittivity (F/m). With increasing frequency,  $dE/dt$  increases and thereby the magnitude of the contribution of the capacitive charging current to the total current increases; in impedance spectroscopy this is observed by a decrease of impedance with increasing frequency. Therefore, the sensitivity coefficient distribution within the measured volume could be derived from the finite-element model with both resistive and capacitive elements presented in this paper.

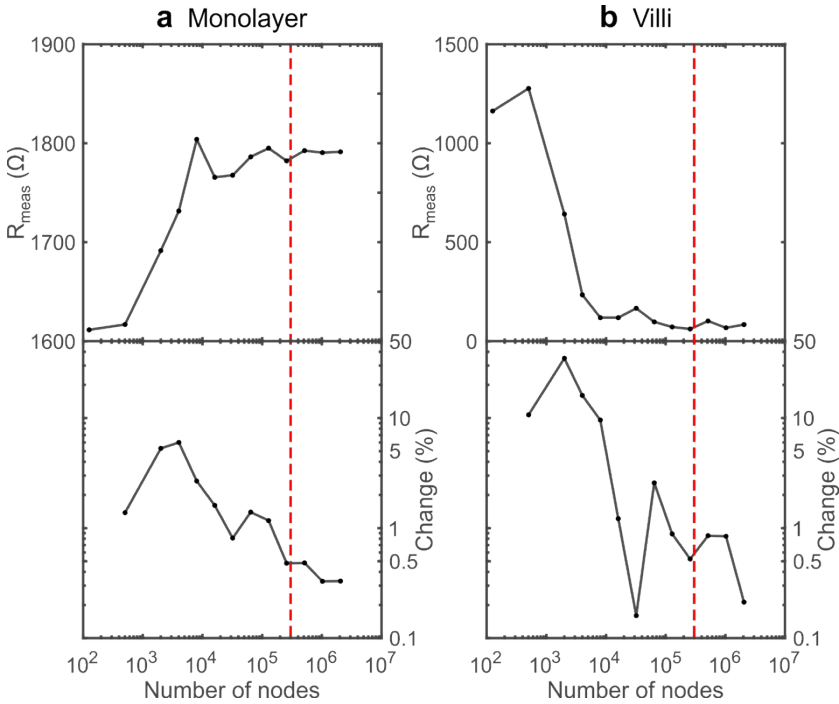
**Supplementary figures**



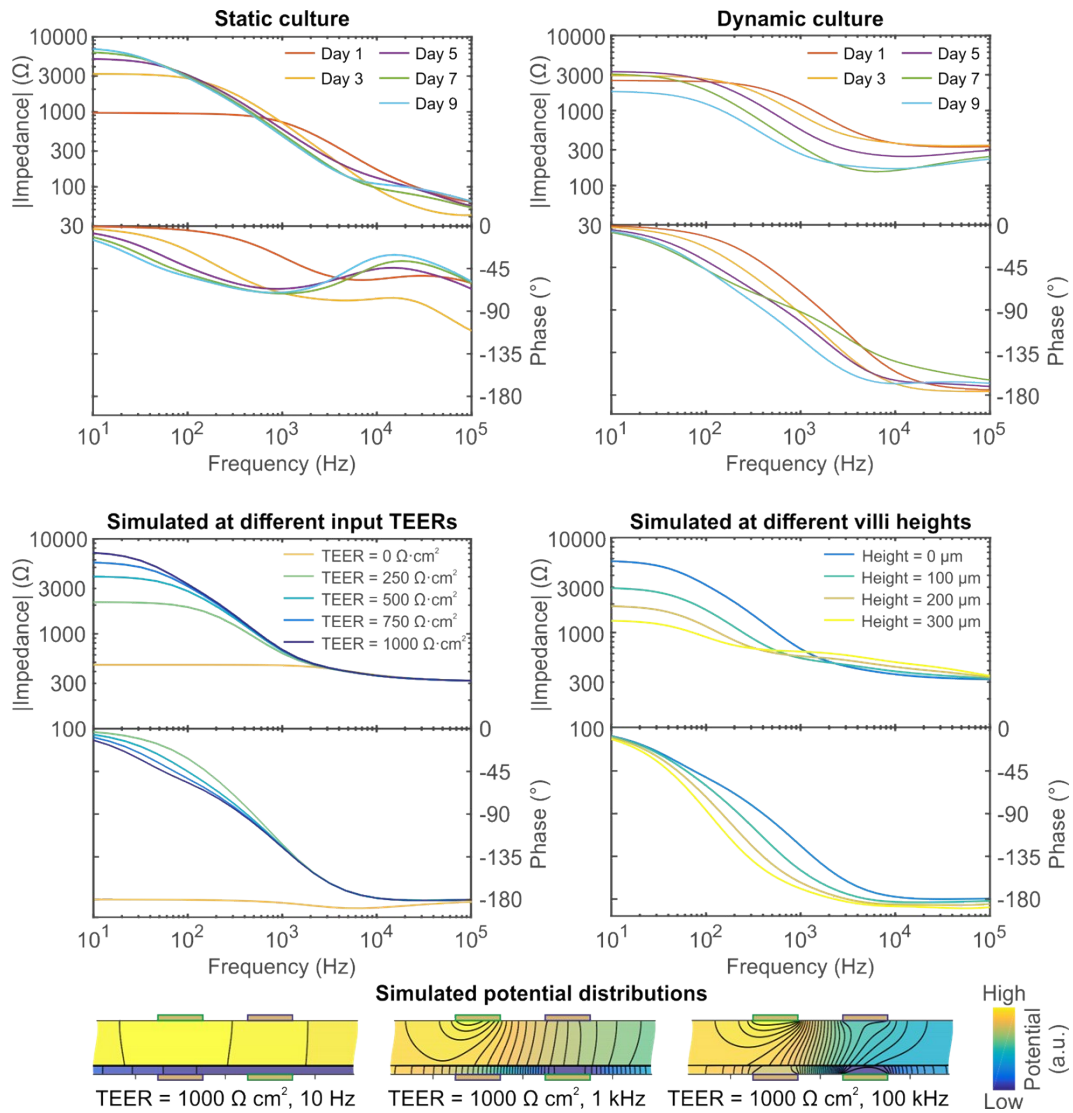
**Supplementary Fig 1** The semi-transparent gold electrodes in the gut-on-a-chip device allow microscopic inspection of the Caco-2 cells cultured between them.



**Supplementary Fig 2** The formation of 3D intestinal villi within the epithelium over time as observed by differential interference contrast (DIC) microscopy.

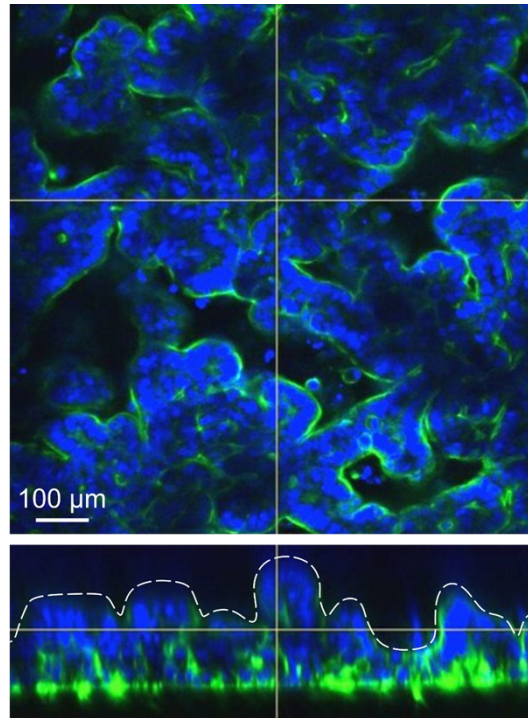


**Supplementary Fig 3** Investigating the convergence of the output parameter  $R_{meas}$  (resistance between readout electrodes resulting from input current and associated electrode potentials). Electrical simulations were performed iteratively, doubling the total number of nodes each time. In the top graphs, the values of output parameter  $R_{meas}$  are displayed. In the bottom graphs, the change (in %) of the current simulation compared to the previous simulation is shown. At approximately 2000 by 144 nodes (~290000, red dashed line) the change between subsequent simulations reaches 0.5%, leading to the conclusion that this is a sufficient amount of nodes to faithfully model the TEER measurements in the gut-on-a-chip. As input parameters a flat monolayer (a) or a monolayer with 250 μm high villi (b) was used, both with a TEER of 1000 Ω-cm<sup>2</sup>, subjected to an AC current of 100 Hz.

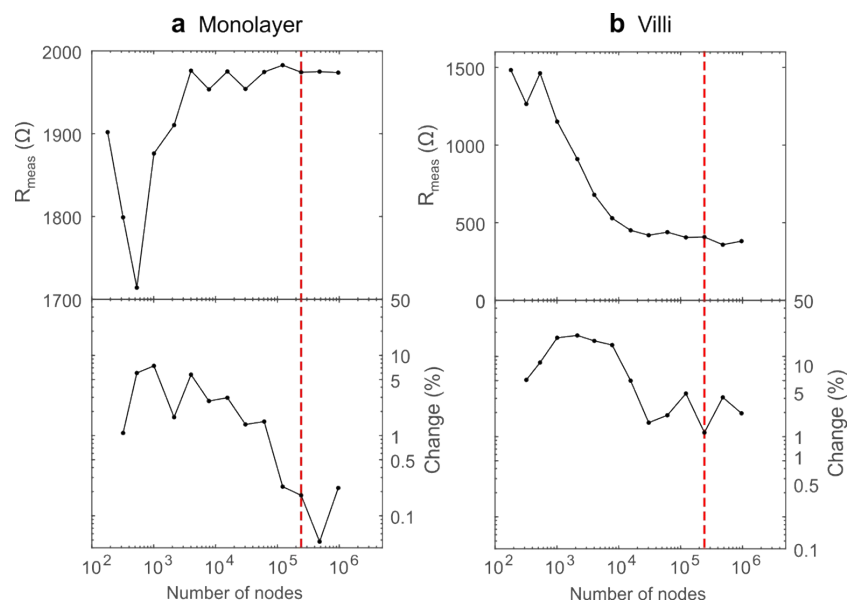


**Supplementary Fig 4** Impedance spectra from the paper accompanied by their phase spectra. It can be seen that both the experimental measurements and the simulations of an electrical network consisting of only resistors and capacitors give rise to  $-180^\circ$  phase shifts. This can be explained by changes in the general direction of the current, which is illustrated using the potential distributions at a TEER of  $1000 \Omega\cdot\text{cm}^2$  that were also shown in the main paper (**Fig. 3a**). When going from 10 Hz to 100 kHz, the polarity of the readout electrodes shifts  $-180^\circ$  due to channel geometry and electrode configuration: the potential of the bottom readout electrode becomes larger than the potential of the top readout electrode, effectively swapping the terminals. This effect, that has also been described by Grimnes and Martinsen,<sup>1</sup> makes these data unsuitable for general impedance fitting methods.

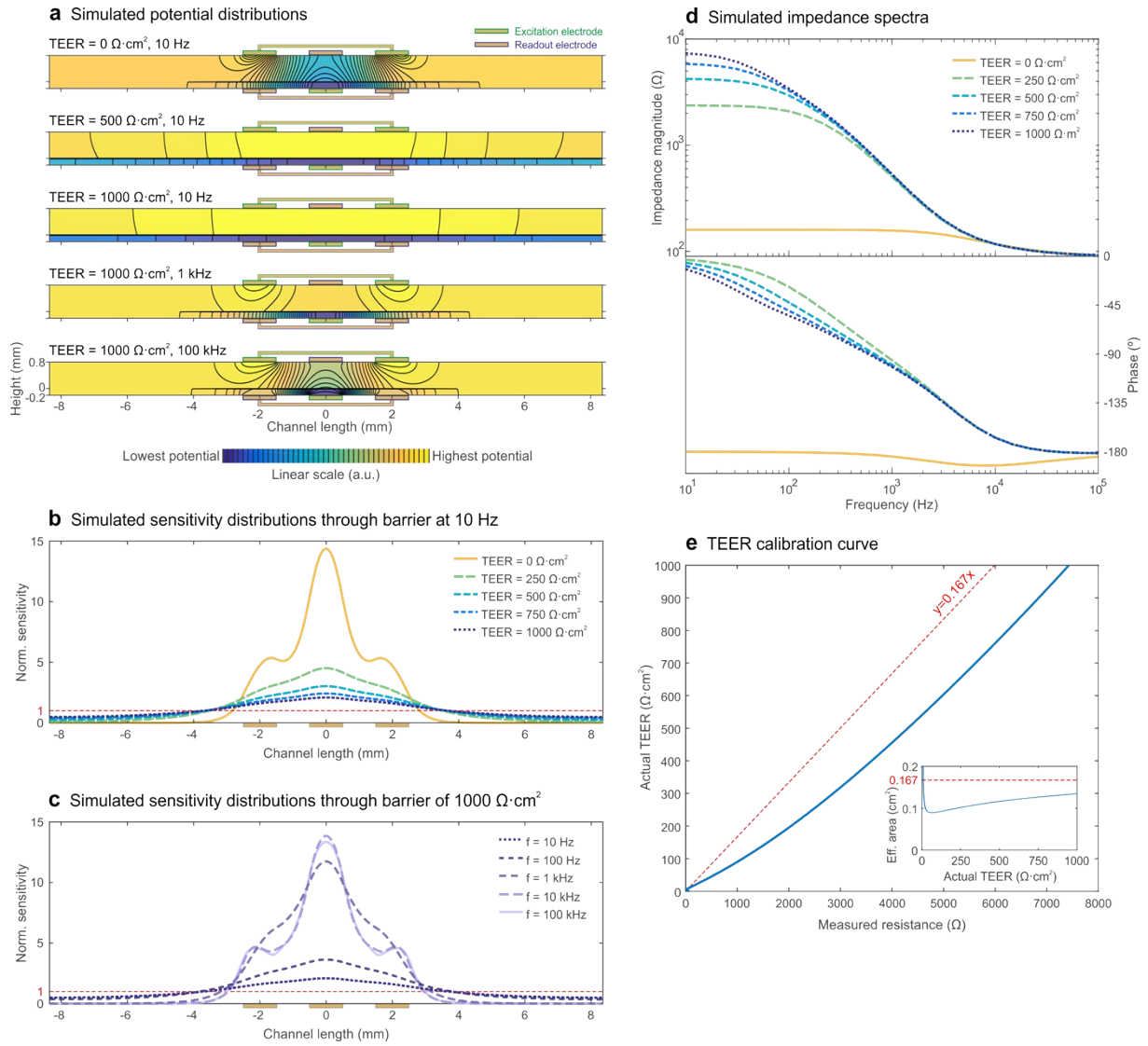




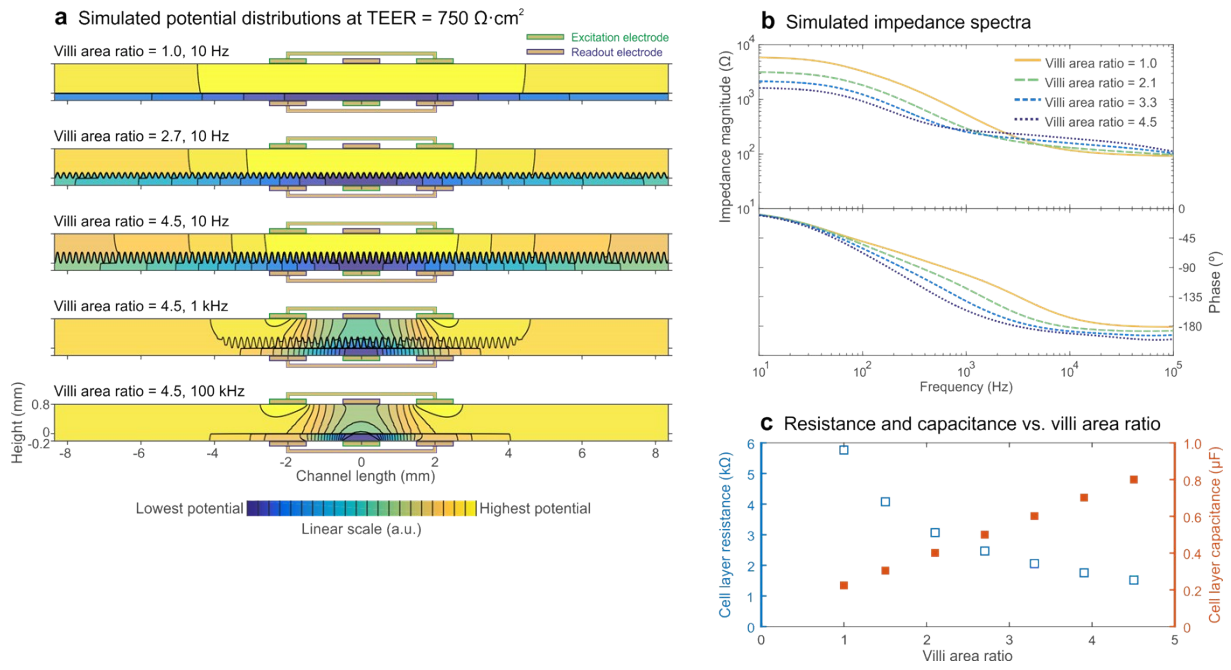
**Supplementary Fig 5** Confocal images of a Caco-2 cell layer cultured under flow for 9 days revealed an approximated villi height of 150  $\mu\text{m}$  to 250  $\mu\text{m}$  and an average inter-villi spacing of 167  $\mu\text{m}$ . Therefore, the sinusoidally modeled villi have a period of 167  $\mu\text{m}$  and a height range of 0  $\mu\text{m}$  (flat monolayer) up to 300  $\mu\text{m}$  (differentiated villi). Blue shows nuclei, green shows actin filaments, scalebar is 100  $\mu\text{m}$ .



**Supplementary Fig 6** Investigating the convergence of the output parameter  $R_{\text{meas}}$ , analogously to **Supplementary Figure 3**. For subsequent simulations networks of 2000 by 120 nodes ( $\sim 240000$ , red dashed line) were used. As input parameters a flat monolayer (**a**) or a monolayer with 250  $\mu\text{m}$  high villi (**b**) was used, both with a TEER of 1000  $\Omega\cdot\text{cm}^2$ , subjected to an AC current of 100 Hz.



**Supplementary Fig 7** Electrical simulations with different input TEERs to model static barrier development in the 6-electrode chip. Note in a that also here electrode polarity inverts at low input TEER or high frequency, corresponding to the  $-180^\circ$  phase shift seen in the impedance spectra.



**Supplementary Fig 8** Electrical simulations with increasing villi area ratio to assess the influence of villi formation on impedance spectra.

## Supplementary tables

**Supplementary Table 1** | TEER of Caco-2 monolayers in Transwell for comparison with TEER in static chips. TEER values were measured at four time points in three wells with Caco-2 barriers, which were allowed to mature for 6 weeks. The average TEER  $\pm$  standard deviation for these twelve measurements was  $736 \pm 120 \Omega \text{ cm}^2$ . Analogously to the chips, TEER was measured using electrical impedance spectroscopy by connecting the same Autolab PGStat12 to the probe cables of an Endohm chamber.

---

6 weeks	+	0 h	1 h	2 h	24 h
Transwell 1		766 $\Omega \cdot \text{cm}^2$	865 $\Omega \cdot \text{cm}^2$	832 $\Omega \cdot \text{cm}^2$	613 $\Omega \cdot \text{cm}^2$
Transwell 2		813 $\Omega \cdot \text{cm}^2$	846 $\Omega \cdot \text{cm}^2$	822 $\Omega \cdot \text{cm}^2$	662 $\Omega \cdot \text{cm}^2$
Transwell 3		792 $\Omega \cdot \text{cm}^2$	676 $\Omega \cdot \text{cm}^2$	679 $\Omega \cdot \text{cm}^2$	460 $\Omega \cdot \text{cm}^2$
Average					736 $\Omega \cdot \text{cm}^2$
Standard deviation					120 $\Omega \cdot \text{cm}^2$

## Supplementary references

1. S. Grimnes and Ø. G. Martinsen, *Journal of Physics D: Applied Physics*, 2007, **40**, 9-14.
2. D. B. Geselowitz, *IEEE Transactions on Biomedical Engineering*, 1971, 38-41.
3. M. Wang, Q. Wang and B. Karki, *Phil. Trans. R. Soc. A*, 2016, **374**, 20150329.
4. P. Metherall, D. Barber, R. Smallwood and B. Brown, *Nature*, 1996, **380**, 509.
5. D. Günzel, S. S. Zakrzewski, T. Schmid, M. Pangalos, J. Wiedenhoef, C. Blasse, C. Ozboda and S. M. Krug, *Annals of the New York Academy of Sciences*, 2012, **1257**, 142-151.
6. J. Golowasch and F. Nadim, in *Encyclopedia of Computational Neuroscience*, eds. D. Jaeger and R. Jung, Springer New York, New York, NY, 2015, pp. 555-558.
7. P. Kauppinen, J. Hyttinen and J. Malmivuo, *International Journal of Bioelectromagnetism*, 2006, **8**, 1-9.